Single-Crystal EPR Study of Triplet Excitons in Tetraethylammonium 2,3,5,6-Tetracyanobenzoquinonide. Evidence for an Interdimer Triplet Exciton

Rosemary C. Hynes,[1a] Paul J. Krusic*,[1b], Keith F. Preston,*,[1a] Jerry J. Springs,[1a] Antony J. Williams,[1a] and Joel S. Miller*,[1b,c]

Contribution from the Steacie Institute for Molecular Sciences, National Research Council of Canada, Ottawa, Ontario, Canada, K1A 0R9,[1d] and the Du Pont Company, Central Research and Development Laboratory, Wilmington, Delaware 19880-0328[1e]

Received June 16, 1994[⊗]

Abstract: EPR spectroscopy of single crystals of tetraethylammonium 2,3,5,6-tetracyano-*p*-benzoquinonide, $([Et_4N]^+)_2[Q]_2^{2-}$, at temperatures near ambient indicates the presence of an electronic triplet species ($S = 1$) exhibiting fine-structure splitting. At 380 K the **g**- and spin–spin interaction matrices were established from measurements of the fine-structure splitting as a function of angle in three orthogonal crystal planes of crystallographically oriented single crystals: **g** = (2.0020, 2.0079, 2.0048); **D** = (−379.6, 243.7, 141.2 MHz). The $\mathbf{g}^2$-tensor is aligned within a few degrees of the local symmetry elements of the constituent $[Q]^-$ anions of the crystal, *i.e.*, perpendicular to the ring, along O–O, and across the ring. Comparison of the eigenvectors of **D** with crystal directions shows that the triplet spectrum is *not* due to intradimer electronic interaction, *i.e.*, interaction associated with the constituents of the $[Q]_2^{2-}$ dimer anion, but rather to interdimer interactions within the anion stack. The change in **D** as a function of temperature is explained in terms of thermal expansion of the crystal. From the temperature dependence of the spectral intensity it is established that the radical pair has a singlet ground state which lies 3075 ± 42 cm^{-1} (8.79 ± 0.12 kcal/mol; 0.381 ± 0.005 eV) below the observed triplet.

Introduction

Through the presence of low-lying empty π-molecular orbitals (LUMO's), planar organic molecules containing strong electronegative groups are often excellent electron acceptors which readily combine with appropriate donors to form ionic solids. Anils[2] and 7,7,8,8-tetracyano-*p*-quinodimethanes[3–17] (TCNQ's) are notable examples which combine with donor molecules to provide a great variety of stable ionic "low-dimensional" or "π-molecular" compounds. Depending on the structure, such materials may exhibit high electrical conductivity[18] and, in a few cases, cooperative magnetic phenomena.[19] The former is associated with the presence of segregated stacks of paramagnetic acceptors and with the electronic interactions therein. The radical anion planes are usually parallel within a stack, but neighbors may be "slipped" with respect to each other. Site inequivalence can result in an alternation in the strength of electronic coupling along the stack so that the unpaired spins are strongly correlated in pairs associated with groups, usually pairs of anions. Such correlated electron pairs, known as Frenkel spin excitons, are coupled antiferromagnetically but usually have thermally accessible triplet states which are detectable by EPR spectroscopy. Subtle changes in crystal structure can profoundly influence the overlap of the π-systems of neighboring anions and hence the electronic and magnetic

⊗ Abstract published in *Advance ACS Abstracts*, February 15, 1995.

(1) (a) National Research Council of Canada. (b) Du Pont. (c) Current address: Department of Chemistry, University of Utah, Salt Lake City, UT 84112. (d) NRCC No. 37276. (e) Contribution No. 5626.

(2) Gordon, D.; Hove, M. J. *J. Chem. Phys.* **1973**, *59*, 3419. Lequan, R.; Lequan, M; Jaouen, G.; Ouahab, L.; Batail, P.; Padiou, J.; Sutherland, R. G. *J. Chem. Soc., Chem. Commun.* **1985**, 116.

(3) Morton, J. R.; Preston, K. F.; Le Page, Y.; Williams, A. J.; Ward, M. D. *J. Chem. Phys.* **1990**, *93*, 2222.

(4) Bandrauk, A. D.; Ishii, K.; Truong, K. D.; Aubin, M.; Hanson, A. W. *J. Phys. Chem.* **1985**, *89*, 1478.

(5) Kepler, R. G. *J. Chem. Phys.* **1963**, *39*, 3528.

(6) Grossel, M. C.; Evans, F. A.; Hriljac, J. A.; Morton, J. R.; Le Page, Y.; Preston, K. F.; Sutcliffe L. H.; Williams, A. J. *J. Chem. Soc., Chem. Commun.* **1990**, 439.

(7) Hynes, R. C.; Morton, J. R.; Preston, K. F.; Williams, A. J.; Evans, F. A.; Grossel, M. C.; Sutcliffe, L. H.; Weston, S. C. *J. Chem. Soc., Faraday Trans.* **1991**, *87*, 2229.

(8) Acker, D. S.; Harder, R. J.; Hertler, W. R.; Melby, L. R.; Benson, R. E.; Mahler, W.; Mochel, W. E. *J. Am. Chem. Soc.* **1960**, *82*, 6408.

(9) Melby, L. R.; Harder, R. J.; Hertler, W. R.; Mahler, W.; Benson, R. E.; Mochel, W. E. *J. Am. Chem. Soc.* **1962**, *84*, 3374.

(10) Vegter, J. G.; Hibma, T.; Kommandeur, J. *Chem. Phys. Lett.* **1969**, *3*, 427.

(11) Chestnut, D. B.; Phillips, W. D. *J. Chem. Phys.* **1961**, *35*, 1002.

(12) Chestnut, D. B.; Arthur, P., Jr. *J. Chem. Phys.* **1962**, *36*, 2969.

(13) Nordio, P. L.; Soos, Z. G.; McConnell, H. M. *Annu. Rev. Phys. Chem.* **1966**, *17*, 237.

(14) Hibma, T.; Dupuis, P.; Kommandeur, J. *Chem. Phys. Lett.* **1972**, *15*, 17.

(15) Hibma, T.; Kommandeur, J. *Phys. Rev. B* **1975**, *12*, 2608.

(16) Silverstein, A. J.; Soos, Z. G. *Chem. Phys. Lett.* **1976**, *39*, 525.

(17) Morton, J. R.; Preston, K. F.; Ward, M. D.; Fagan, P. J. *J. Chem. Phys.* **1989**, *90*, 2148.

(18) For a detailed overview, see the proceedings of the recent series of international conferences: *Synth. Met.* **1993**, *55–57* (Stafström, S., Saleneck, S. R., Inganäs, O., Hjertberg, T., Eds.); *Synth. Met.* **1991**, *41–43* (Hanack, M., Roth, S.. Schier, H., Eds.); *Synth. Met.* **1988**, *27*; **1989**, *28*, *29* (Aldissi, M., Ed.); *Mol. Cryst. Liq. Cryst.* **1985**, *117–121* (Pecile, C., Zerbi, G., Bozio, R., Girlando, A., Eds.); *J. Phys. (Paris) Colloq.* **1983**, *44-C3* (Comes, R., Bernier, P., André, J. J., Rouxel, J., Eds.); *Mol. Cryst. Liq. Cryst.* **1981**, *77*, *79*, *82*, *83*, *85*; **1982**, *86* (Epstein, A. J., Conwell, E. M., Eds.); *Chem. Scr.* **1981**, *17* (Carneiro, K., Ed.); *Lecture Notes in Physics* **1979**, *95*, *96* (Bartsic, S., Bjelis, A., Cooper, J. R., Leontic, B. A., Eds.); *Ann. N. Y. Acad. Sci.* **1978**, *313* (Miller, J. S., Epstein, A. J., Eds.).

(19) Review papers: Miller, J. S.; Epstein, A. J. *Angew. Chem. Int. Ed. Engl.* **1994**, *33*, 385. Buchachenko, A. L. *Russ. Chem. Rev.* **1990**, *59*, 307; *Usp. Khim.* **1990**, *59*, 529. Kahn, O. *Struct. Bonding* **1987**, *68*, 89. Kahn, O.; Journaux, Y. In *Inorganic Materials*; Bruce, D. W., O'Hare, D., Eds.; J. Wiley & Sons: New York, 1993, 59. Caneschi, A.; Gatteschi, D.; Sessoli, R.; Rey, S. *Acc. Chem. Res.* **1989**, *22*, 392. Miller, J. S.; Epstein, A. J.; Reiff, W. M. *Acc. Chem. Res.* **1988**, *21*, 114. Miller, J. S.; Epstein, A. J.; Reiff, W. M. *Science* **1988**, *240*, 40. Miller, J. S.; Epstein, A. J. In *New Aspects of Organic Chemistry*; Yoshida, Z., Shiba, T., Ohsiro, Y., Eds.; VCH: New York 1989; 237. Epstein, A. J.; Miller, J. S. *Mol. Cryst. Liq. Cryst.* **1993**, *228*, 99.

0002-7863/95/1517-2547$09.00/0

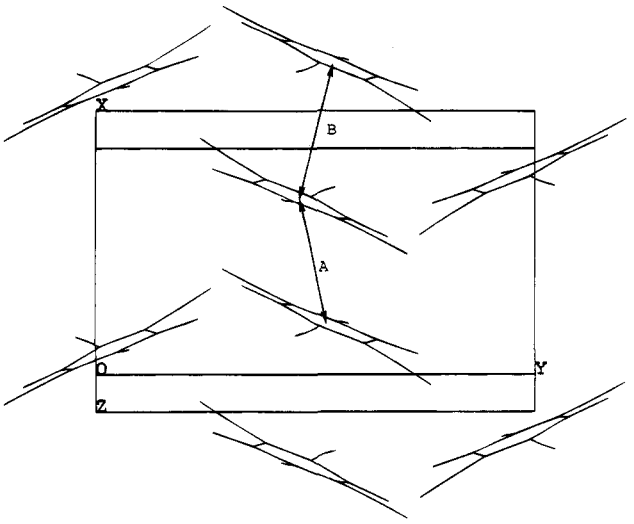

Figure 1. Crystallographic unit cell of $([Et_4N]^+)_2[Q]_2^{2-}$ showing anion locations and the interacting pairs ***A*** and ***B***.

properties of this class of materials. Our research interests are directed toward a better understanding of this unusual class of solids and their use as solid-state devices.

Single-crystal EPR spectroscopy is a particularly valuable tool in the investigation of magnetic interactions since it provides the tensor principal directions which are pivotal in the location of unpaired spin and the assignment of ground-state geometries and electronic structures. In studies of low-dimensional solids, it can often be used to advantage to identify the radical pairs that are responsible for the magnetic behavior. Herein we discuss the EPR spectroscopy of the low-dimensional compound tetraethylammonium 2,3,5,6-tetracyanobenzoquinonide, $([Et_4N]^+)_2[Q]_2^{2-}$, whose synthesis and X-ray structural characterization have been reported.[20] One-dimensional chains of the dimers $[Q]_2^{2-}$ are evident in the crystal structure (Figure 1) in which the anion separations (centroid-to-centroid) alternate between 3.52 (***A***) and 3.91 Å (***B***) (or 2.84 and 3.51 Å, plane-to-plane). EPR powder spectra of the material suggest the presence of only one triplet interaction ($S = 1$) but do not, of course, permit a definitive assignment of the spin carrier to pairs of anions. The ***A*** dimer, Figure 1, has been identified as a strong dimer, $([Et_4N]^+)_2[Q]_2^{2-}$, through considerations of proximity and geometry of its constituents.[20] Our single-crystal EPR study, however, leads to an unambiguous conclusion that the ***A*** dimer is not EPR-active; instead, we find that the observed spin–spin triplet interaction has a principal axis that precisely aligns with the vector ***B*** and is associated with an interdimer interaction.

Experimental Section

The mono(*N,N,N*-triethylethanaminium) salt of 4-hydroxy-2,3,5,6-tetracyanophenoxy (tetraethylammonium 2,3,5,6-tetracyanoquinonide), $([Et_4N]^+)_2[Q]_2^{2-}$, was synthesized as described previously.[20] Red needle single crystals were obtained by recrystallization from acetonitrile and belong to the monoclinic *P2/n* space group.[20] Single crystals were oriented absolutely on a Nonius diffractometer according to the structural parameters. Oriented crystals were sealed into the ends of 4 mm quartz tubes with epoxy glue such that each of the three standard orthogonal axes *a**, *b*, and *c* in turn was aligned along the tube axis. A pointer, mounted at right angles to the tube, indicated the direction of a second orthogonal axis. The oriented crystals were positioned in a Dewar insert at the center of the E-321 resonant microwave cavity of a Varian Associates E-12 X-band EPR spectrometer. The sample temperature was maintained at 380 K by a Lake Shore Cryotronics 805 controller equipped with a silicon diode temperature sensor.

The dc magnetic field intensity was measured with a Bruker ER-035M NMR gaussmeter, and the microwave frequency was determined using a Systron-Donner digital counter. The axis of the sample tube was held perpendicular to the magnetic field $\mathbf{B}_o$ of the spectrometer, while a horizontal brass protractor graduated every 5° of arc measured the angle between the magnetic field and a pointer affixed to the sample tube. By rotation of the sample tubes about their axes it was possible to explore each of the three crystal planes *a*b*, *a*c*, and *bc*. EPR spectra at 380 K were recorded at intervals of 10 or 15° throughout each of these planes.

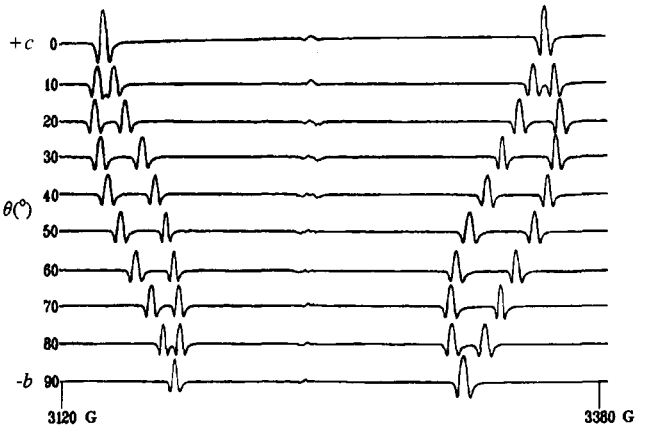

Figure 2. Second derivative EPR spectrum as a function of angle in the *bc* plane at 380 K and 9095 MHz.

Results

Above ca. 300 K a single crystal of $([Et_4N]^+)_2[Q]_2^{2-}$ at an arbitrary orientation in the dc magnetic field shows (Figure 2) two pairs of intense EPR absorptions ($\Delta B_{pp} \approx 1$ G) almost symmetrically disposed about an additional weak absorption close to the free-spin *g*-factor (2.0023). The central feature splits into two lines for certain orientations but shows only weak anisotropy; the stronger resonances are highly anisotropic, however, and "cross" for certain orientations (Figure 3). Such crossings are characteristic of a triplet interaction ($S = 1$) in a single crystal and correspond to a change in sign for the separation of the $\Delta m_S = \pm 1$ resonances.[21] Doubling of the lines in the EPR spectrum and the pattern of coalescences (Figure 3) are typical of the "site-splitting" behavior of paramagnets in a monoclinic crystal.[22] The sites responsible for both weak and strong resonances evidently conformed with the crystal space group of the host. The variation in magnetic field splitting (ΔB) for the triplet pairs was analyzed according to the Hamiltonian[21]

$$\mathrm{H} = \beta \mathbf{H}\cdot\mathbf{g}\cdot\mathbf{S} + \mathbf{S}\cdot\mathbf{D}\cdot\mathbf{S}$$

where the symbols have their usual meanings. Since the fine-structure contribution ($\mathbf{S}\cdot\mathbf{D}\cdot\mathbf{S}$) was clearly much smaller than the electronic Zeeman term ($\beta\mathbf{H}\cdot\mathbf{g}\cdot\mathbf{S}$), a first-order treatment[21] was appropriate. Scalar values of $\boldsymbol{l}\cdot\mathbf{g}\cdot\mathbf{D}\cdot\mathbf{g}\cdot\boldsymbol{l}$ were calculated for each direction $\boldsymbol{l}$ within a crystal plane by using the approximate expression $g^3\beta\Delta B/3$ for each pair of triplet lines. The appropriate *g*-factor was determined from the associated weak central features.

Plots of $g^3\beta\Delta B/3$ and of g^2 against angle were made for each of the orthogonal planes (Figure 3), and least-squares procedures were used to extract the best estimates of the elements of the $\mathbf{g}\cdot\mathbf{g}$ and $\mathbf{g}\cdot\mathbf{D}\cdot\mathbf{g}$ matrices.[22] Diagonalization procedures led to the

(20) Vasquez, C.; Calabrese, J. C.; Dixon, D. A.; Miller, J. S. *J. Org. Chem.* **1993**, *58*, 65.

(21) Pake, G. E.; Estle, T. L. In *The Physical Principles of Electron Paramagnetic Resonance*; Benjamin, Inc.: Reading, MA, 1973; Chapter 5.

(22) Morton, J. R.; Preston, K. F. *J. Magn. Reson.* **1983**, *52*, 457.

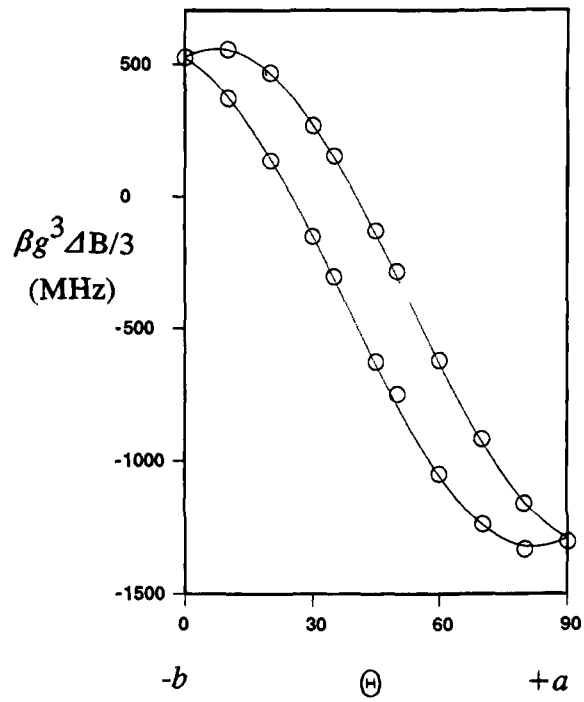

Figure 3. Example of sinusoidal dependence of l·g·D·g·l on angle within a crystal plane. Plot of $\beta g^3 \Delta B/3$ versus angle for the a^*b plane and least-squares best-fit sine curve.

Table 1. Experimental g^2 and **g**·**D**·**g** Tensors[a] for $([Et_4N]^+)_2[Q]_2^{2-}$, Principal Values of **g** and **D** in MHz, and their Direction Cosines in the a^*bc Crystal Axis System[b] at 380 K

				principal values and direction cosines of **g** and **D**		
	Tensor[c]			*x*	*y*	*z*
				g =	**g** =	**g** =
	*a**	*b*	*c*	2.0048	2.0079	2.0020
g^2	4.0107	−0.0073	−0.0001	0.2287	−0.3110	−0.9225
	−0.0073	4.0273	0.0043	−0.2835	0.8852	−0.3687
	−0.0001	0.0043	4.0205	0.9313	0.3459	0.1143

				principal values and direction cosines of **g** and **D**[d]		
	Tensor[c]			**D** =	**D** =	**D** =
	*a**	*b*	*c*	243.7	141.2	−379.6
g·**D**·**g** (MHz)	−1324.3	−246.6	−614.3	−0.2483	−0.1444	0.9579
	−246.6	537.9	−100.6	−0.0832	0.9883	0.1274
	−614.3	−100.6	812.8	0.9651	0.0481	0.2574

[a] Tensor determined from measurements of $g^3\beta\Delta B/3$ (in MHz) with g taken to be that for the central resonance, β = 1.399610877 MHz/G. [b] a^* is the vector product of the crystal axes b and c. [c] Tensor for one site only; second-site parameters obtained by changing signs of a^*b and bc elements of tensor and b-component of the directional cosines. [d] Only the relative signs of D_{xx}, D_{yy}, and D_{zz} can be determined. The absolute signs given here are chosen to agree with theory.

principal values and their direction cosines for both **g** and **D** (Table 1). The zero-field parameters[23] D and E obtained from the principal values of **D** are:

$$D = 3D_{zz}/2 = -569.4 \text{ MHz}$$

$$E = (D_{xx} - D_{yy})/2 = 51.2 \text{ MHz}$$

The absolute signs of the **D** components could not be determined from the EPR experiment; they were chosen to give the negative value of D anticipated for pure dipolar interaction between two electrons.

(23) Atherton, N. M. *Electron Spin Resonance*; Horwood: Chichester, UK, 1973; Chapter 5.

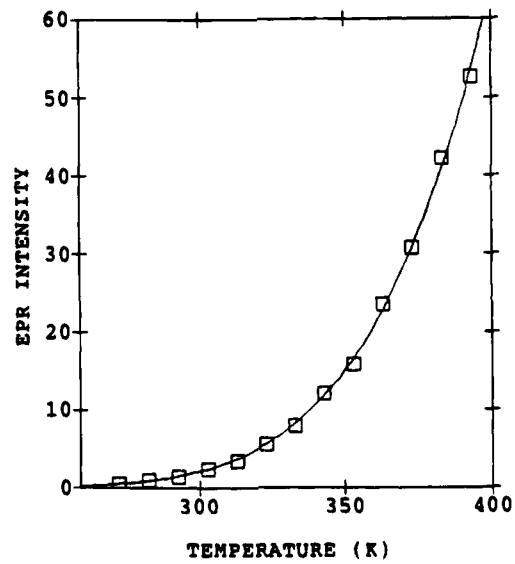

Figure 4. Temperature dependence of the spectral intensity, I, of the triplet for a random orientation of the crystal. Least-squares fit to intensity, $I = \{T[\exp(J/k_BT) + 3]\}^{-1}$.

The temperature dependence of the triplet spectral intensity was established from measurements taken every 10 K over the range 270−390 K for an orientation where the four intense lines of the site-split spectrum were well-separated. The microwave power was reduced to a minimum in these measurements to prevent saturation, and the line intensities, I, were obtained by electronic integration. An expression of the form[24]

$$I \propto 1/\{T[\exp(J/k_BT) + 3]\}$$

which describes the temperature dependence of the EPR spectrum of a thermally activated triplet, was fit to the data (Figure 4) by a generalized least-squares method. The singlet−triplet energy spacing, ΔE_{st}, estimated from this treatment was 3075 ± 42 cm^{-1} (8.79 ± 0.12 kcal/mol; 0.381 ± 0.005 eV).

Discussion

The orientation dependence of the strong EPR spectrum and the temperature dependence of its intensity verify the existence of a thermally excited electronic triplet in the crystal of $([Et_4N]^+)_2[Q]_2^{2-}$. The small anisotropy in **g** and the proximity of its trace to the free spin g-factor suggest that the triplet spectrum arises from the interaction between a pair of organic radicals. Closer inspection of both **g** and **D** shows that the triplet is, in fact, associated with the tetracyanoquinoidal constituents $[Q]^-$ intrinsic to the crystal. The appearance of weak absorptions (Figure 2) at the center of the triplet spectrum is associated with traces of $S = {}^1/_2$ "unpaired" $[Q]^{\bullet-}$ or $[Q]_2^{\bullet-}$ defects with the same **g**-matrix.

The principal directions of **g** correlate well with the three 2-fold axes of the pseudo-D_{2h} $[Q]^-$ unit in $[Q]_2^{2-}$ (Figure 5). The **g**-component closest to the free-spin value, g_{min}, lies only 3.0° from the perpendicular to the least-squares plane (0.9041, 0.3988, −0.1533) of the $[Q]^-$ unit; g_{max} lies only 2.6° from the long axis of $[Q]^-$, *i.e.*, the O−O vector; and g_{int} lies 3.7° from the other 2-fold axis within the $[Q]^-$ plane. This alignment of **g** with the symmetry elements of the $[Q]^-$ unit is anticipated for a π-radical.[25] Furthermore, the small shifts of the g-values from that of free spin and the alignment of the component closest to free spin with the perpendicular to the ring are typical of a

(24) Bijl, K.; Kainer, H.; Rose-Innes, A.-C. *J. Chem. Phys.* **1959**, *30*, 765.

(25) Morton, J. R. *Chem. Rev.* **1964**, *64*, 453.

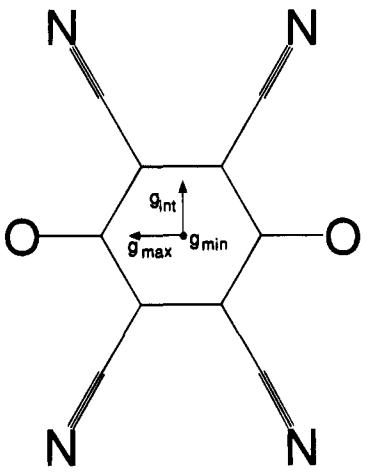

Figure 5. The association of principal g-values with directions within the anion.

Table 2. Comparison of Experimental D_{zz} Eigenvector with Center–Center Vectors of Intrinsic Radical Pairs *A* and *B*

	a^*	b	c	θ, deg[a]
D_{zz}	0.9579	±0.1274	0.2574	
radical Pair *A* (3.52 Å apart)[b]	0.9089	±0.2015	−0.3650	36.6
radical Pair *B* (3.91 Å apart)[b]	0.9518	±0.1811	0.2475	3.1

[a] Smallest angular separation from principal direction of maximum **D** component. [b] Center–center vector connecting two $[Q]^-$ rings within the crystal.

π-radical.[25] Therefore, there can be little doubt that the electronic Zeeman interaction in both the intense $S = 1$ and the weak $S = {}^1/_2$ sites is due to the intrinsic tetracyanoquinoidal units.

Unfortunately, the magnitude alone of the zero-field D parameter ($|D| = 569.4$ MHz) is insufficient to identify the $[Q]^-$ units that are the carriers of the observed triplet interaction. If the interaction were between two localized electrons, their separation r could be estimated, knowing D, from the expression[26]

$$\langle r \rangle = \left(\frac{12\,980}{2|D|} \left\{ 2g_{zz}^2 + \frac{g_{yy}^2}{2} + \frac{g_{xx}^2}{2} \right\} \right)^{1/3}$$

where r is in Å and D in MHz. For delocalized unpaired electrons, however, the single distance r derived from this expression has no significance. Consequently, the value of $r = 5.16$ Å derived for the present example casts little light on the origin of the triplet interaction. Much more revealing, however, is a comparison of the principal direction of the maximum absolute component of the **D** tensor with the center-to-center vectors *A* and *B* separating adjacent $[Q]^-$ units (Figure 1, Table 2). The vector *B* for the pair of $[Q]^-$ units separated by the greater distance lies only 3.1° from the D_{zz} eigenvector while the vector *A* for the closer pair does not correlate at all with the direction of the D_{zz} tensor component (36.6°). Thus, the observed triplet cannot be associated with the constituents of the $[Q_2]^{2-}$ dimer but rather with interacting unpaired electron distributions associated with the more distant *B* pair of $[Q]^-$ units. A detailed calculation of the dipolar interaction expected for a model consisting of two $[Q]^-$ anion radicals units oriented exactly as pair *B* confirms this assignment.

Simple valence-bond considerations of *p*-benzoquinone anion radicals suggest that the unpaired electron resides mostly on the two oxygen atoms in $2p_z$ orbitals directed perpendicular to the anion plane. STO-3G/UHF MO calculations for $[Q]^-$, although showing delocalization over the entire radical, do not change appreciably this picture and place the majority of the unpaired electron density on the two oxygens.[20] Using the approximation that the unpaired spin density is evenly split on each $2p_z$ orbital of the oxygen atoms, we have computed dipolar tensors for pairs of $[Q]^-$ radicals oriented as the *A* and *B* pairs of $[Q]^-$ units in the crystal from the anisotropic part of the tensor[26]

$$0.5\beta \sum_{i,j} \varrho_i \varrho_j r_{ij}^{-3} \{ \mathbf{g}\cdot\mathbf{g} - 3\cdot(\mathbf{g}\cdot\mathbf{r})(\mathbf{g}\cdot\mathbf{r}) \}$$

where β is the Bohr magneton, ϱ_i and ϱ_j are the unpaired spin densities on atoms separated by distance r_{ij} along the direction **r**. The calculations (Table 3) were carried out for the experimental **g**-matrix and for unit cell parameters at the temperature of the measurement (380 K) obtained by quadratic interpolation of the data given in Table 4. Agreement with the experimental spin–spin interaction matrix is very good for the *B* pair but unacceptably poor for the closest pair, *A*. This is particularly true of the largest absolute component, D_{zz}, and its direction cosines: for *B*, the agreement is to within 8% for the values and to within 4° for the direction cosines; pair *A*, however, yields a maximum absolute principal value some 51%

(26) Derived from expressions given in: Abragam, A.; Bleaney, B. *Electron Paramagnetic Resonance of Transition Ions*; Clarendon: Oxford, 1970; pp 492–494.

Table 3. Comparison of Experimental and Calculated[a] Fine-Structure Tensors for $([Et_4N]^+)_2[Q]_2^{2-}$, their Principal Values in MHz, and Direction Cosines in the a^*bc Crystal Axis System[b]

	tensor[c]			principal values and direction cosines of **D** (MHz)		
				x	y	z
				D =	**D** =	**D** =
	a^*	b	c	243.7	141.2	−379.6
Expt.	−330.3	−61.5	−153.0	−0.2483	−0.1444	0.9579
	−61.5	133.5	−25.3	−0.0832	0.9883	0.1274
	−153.0	−25.3	202.2	0.9651	0.0481	0.2574
	tensor[c]			principal values and direction cosines of **D** (MHz)		
				x	y	z
				D =	**D** =	**D** =
	a^*	b	c	419.1	154.5	−573.2
A[a]	−406.1	140.0	310.6	0.2919	0.3369	−0.8952
	140.0	132.2	−138.5	−0.2965	0.9217	0.2501
	310.6	−138.5	274.2	0.9093	0.1924	0.3690
	tensor[c]			principal values and direction cosines of **D** (MHz)		
				x	y	z
				D =	**D** =	**D** =
	a^*	b	c	214.0	139.2	−352.1
B[a]	−305.0	−85.7	−119.6	−0.1310	−0.2758	0.9523
	−85.7	135.7	−51.8	−0.4437	0.8753	0.1924
	−119.6	−51.8	170.4	0.8866	0.3973	0.2370

[a] Tensors calculated for dipolar interaction between nearest neighbors $[Q]^-$ in pairs **A** and **B** for the assumption of unpaired spin densities of 0.5 on each O atom. [b] a^* is the vector product of the crystal axes b and c. [c] Tensor in units of MHz for one site only; second-site parameters obtained by changing signs of a^*b and bc elements of tensor and b-component of direction cosines.

Table 4. Unit Cell Parameters[a] as a Function of Temperature

temperature, K	a, Å	b, Å	c, Å	β, deg
203	6.937	11.755	21.654	92.589
243	6.972	11.777	21.687	92.571
273	7.004	11.782	21.717	92.559
333	7.060	11.820	21.750	92.290
393	7.150	11.830	21.880	92.090

[a] Unit cell remained monoclinic over temperature range.

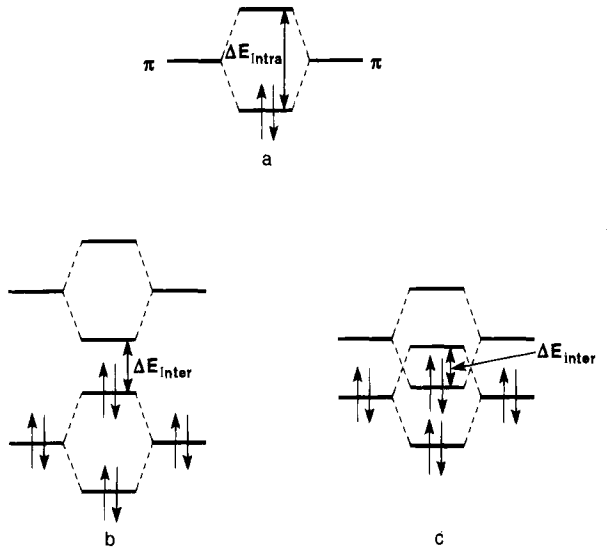

Figure 6. Schematic illustration of the LUMO's overlapping for $[\mathbf{Q}]_2^{2-}$ (a) and a pair of $[\mathbf{Q}]_2^{2-}$'s (b and c).

too large which lies 43° away from the experimental principal direction. Calculations for ***B*** for the remaining two principal values and their directions were in much poorer accord with experiment. The asymmetry of the tensor was underestimated, a failing noticed in similar calculations for $[TCNQ]_2^{2-}$,[6,7] and the principal directions were 22° off target. Nevertheless, the excellent agreement between experimental and calculated D_{zz} values and direction cosines for this simple model convinces us that the assignment of the triplet to interacting unpaired spin distributions associated with the more distant pair of $[\mathbf{Q}]^-$ units (***B***) in the crystal is correct.

The $[\mathbf{Q}]^-$ units in $([Et_4N]^+)_2[\mathbf{Q}]_2^{2-}$ form segregated stacks (Figure 1) in which the constituents are alternately separated along the line joining their centers by 3.52 (pair ***A***) and 3.91 Å (pair ***B***). The formation of a triplet between the more remote pair of anions, rather than within the crystallographically established dimer, is surprising but not unprecedented.[16] Typically, in one-dimensional chains of radicals with disparate spacing between constituent radicals, the triplet exciton is clearly associated with dimers consisting of pairs of *nearest* neighbor radical anions.[3,6,7] However, in phase I of Rb[TCNQ][16] the comparison of experimental and theoretical D and E values and directions reveals that the triplet resides within the pair of $[TCNQ]^{\bullet -}$ within the stack that have the next nearest separation. This observation was rationalized in terms of a better ring-to-external-bond overlap in the favored pair.[16] In the present case of a much more localized unpaired electron, we would expect direct ring overlap to play a dominant role in triplet formation; the rings of the $[\mathbf{Q}]^-$ units of the more distant pair ***B*** are better aligned with each other than the closer pair ***A*** (Figure 1) so that $\pi-\pi$ overlap of the p orbitals and electron exchange are enhanced in the more remote pair. An alternative, but less compelling, point of view is to consider an interdimer interaction schematically illustrated in Figure 6. Strong interaction in the dimer with separation ***A*** forms bonding and antibonding orbitals with a singlet−triplet separation energy of ΔE_{intra} (Figure 6a). The latter is too large for the triplet to be thermally populated at the temperature of the experiments. These dimers can interact with each other via the schemes of either parts b or c of Figure 6 to form a pair each of bonding and antibonding orbitals with singlet−triplet separation energy of ΔE_{inter} which is smaller than ΔE_{intra} to allow thermal population of a triplet state. Such a model would only be consistent with the experimental D value if the unpaired spin were appreciably localized in each component of the pair of dimers.

Table 5. Temperature Dependence of ΔB_{zz}[a]

temperature, K	ΔB (G)	temperature, K	ΔB (G)
319.2	402.6	357.2	396.3
328.7	401.3	366.2	393.7
338.2	399.7	375.2	390.6
347.2	398.4		

[a] Separation in G of outermost lines for a crystal aligned crystallographically such that $\mathbf{B}_o||D_{zz}$ as determined from 380 K data (Table 1); ν = 9117 MHz.

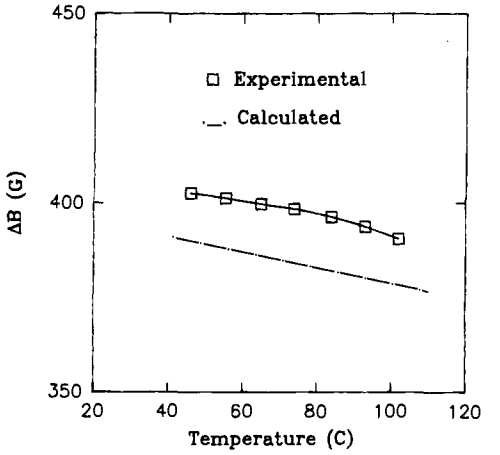

Figure 7. Calculated and experimental values of ΔB_{zz} as a function of temperature.

Observation of the triplet splitting for a fixed orientation of the crystal indicated that it was quite dependent on temperature. In order to examine this dependence quantitatively, a single crystal was aligned along the principal direction for D_{zz} at 380 K, *i.e.*, the direction corresponding to the maximum splitting as determined from the experimental dipolar tensor. (A small systematic error was undoubtedly introduced here since the X-ray alignment was performed at room temperature, whereas the **D** matrix was established at 380 K.) The fine-structure splitting ΔB_{zz} was then determined at intervals of about 10 K throughout the temperature range where the triplet was detectable (Table 5).

It is clear from Table 5 and Figure 7 that ΔB_{zz}, and hence D_{zz}, decreases with increasing temperature, an effect which is readily accounted for in terms of the thermal expansion of the crystal lattice. Theoretical values of ΔB_{zz} were calculated every 10° from 40 to 110 °C using the classical pairwise point-dipolar approximation for the ***B*** dimer, as outlined above, and unit cell parameters interpolated from the data of Table 4 assuming a quadratic temperature dependence for all parameters. Figure 7 compares the experimental and predicted temperature dependences of ΔB_{zz}. It was assumed that the fractional coordinates for the $([Et_4N]^+)_2[\mathbf{Q}]_2^{2-}$ structure did not change with temperature. Even though absolute agreement between calculated and experimental values was not achieved, it is clear that the trend in D_{zz} with temperature is adequately explained in terms of thermal expansion of the unit cell. Failure to reproduce the slight downward curvature evident in the experimental plot may arise from an imperfect alignment of the crystal along z for all temperatures studied.

Conclusions

Single-crystal measurements of the spin−spin interaction tensor clearly show that, quite unexpectedly, the thermally populated electronic triplet in $([Et_4N]^+)_2[\mathbf{Q}]_2^{2-}$ is not associated with the crystallographically established strong ***A*** $[\mathbf{Q}]_2^{2-}$ dimer. Classical point-dipolar calculations for a delocalized unpaired

electron distribution in each of the constituents $[\mathbf{Q}]^-$ of the dimers strongly suggest that the triplet is associated with the next nearest pair ***B*** in the segregated stacks of $[\mathbf{Q}]^-$ units. The preference for localization of the triplet exciton on the more remote pair is attributed to a much better $\pi-\pi$ overlap between the constituent anions. A model which reconciles the seemingly inconsistent crystallographic and spectroscopic observations is that of a triplet dimer of $[\mathbf{Q}_2]^{2-}$ dimers.

Acknowledgment. We would like to thank Mr. Carlos Vasquez (DuPont) for preparing $([Et_4N]^+)_2[\mathbf{Q}]_2^{2-}$ and Mr. William J. Marshall (DuPont) for measurements of the unit cell parameters as a function of temperature. We are also indebted to Dr. David A. Dixon (DuPont) for discussions and to Mr. Regent Dutrisac (NRC) and Mr. Steve Hill (DuPont) for technical assistance.

Supplementary Material Available: Program DIPOLE.BAS for calculating dipolar tensors for point charges (6 pages). This material is contained in many libraries on microfiche, immediately follows this article in the microfilm version of the journal, can be ordered from the ACS, and can be downloaded from the Internet; see any current masthead page for ordering information and Internet access instructions.

JA941903T